Marine and Petroleum Geology 99 (2019) 175–189

Contents lists available at ScienceDirect

Marine and Petroleum Geology

journal homepage: www.elsevier.com/locate/marpetgeo

Research paper

Influence of faults and slumping on hydrocarbon migration inferred from 3D seismic attributes: Sanriku-Oki forearc basin, northeast Japan

Chandoeun Eng[a], Takeshi Tsuji[a,b,*]

[a] Department of Earth Resources Engineering, Kyushu University, 744 Motooka Nishi-ku, Fukuoka 819-0395, Japan
[b] International Institute for Carbon-Neutral Energy Research (I2CNER), Kyushu University, 744 Motooka Nishi-ku, Fukuoka 819-0395, Japan

ARTICLE INFO

Keywords:
Gas accumulation
Gas migration
Coal-bearing strata
Seismic attributes
Forearc basin
Slump
Gas chimney
Faults

ABSTRACT

Seismic imaging of the Sanriku-Oki forearc basin in the Japan Trench plate convergent margin provides insights into the geological controls on hydrocarbon systems in sediment deposited on the continental slope. We perform a series of seismic attribute analyses on 3D seismic reflection data to better define the influence of geological structures (e.g., faults, slumps and gas chimneys) on hydrocarbon sources, migration pathways and reservoirs. In order to identify coal-bearing strata from the 3D seismic volume, we calculate acoustic impedance distribution by integrating seismic and logging data via waveform inversion. Two Late Oligocene to Early Miocene major coal-bearing strata are characterized as low acoustic impedance strata. Gas-bearing strata characterized by anomalously high reflection strength are widely distributed beneath a bottom simulating reflector (BSR). A greater accumulation of gas occurs in the northeast of the study area, where successive slump deposits and gas chimneys are observed. We propose that a BSR with an underlying gas accumulation in the Sanriku-Oki forearc basin developed as a consequence of the expulsion of gas from Cretaceous to Oligocene coal beds and their subsequent upward migration through gas chimneys and faults. Furthermore, the migration and accumulation of gas and gas hydrate were strongly controlled by a series of porous slump deposits. As chimneys and gas pockets occur above the edges of the slumps, gas migration processes controlled by the slumps could be important in the forearc basin. Our study based on seismic attribute analyses demonstrates that features produced by tectonic movements at plate subduction margins (e.g., faults) and associated instability processes (e.g., slumps) represent important controls on the migration and accumulation of hydrocarbons in forearc basins.

1. Introduction

Gas hydrate and free gas in marine sediments account for a large proportion of known natural hydrocarbon gas accumulations (Judd, 2003; Kvenvolden, 1993). Gas hydrate forms as a solid compound binding water and gas molecules, which is stable at the high pressures and low temperatures found in permafrost regions and in deep water sediments (Kinoshita et al., 2011; Berndt et al., 2002; Holbrook et al., 1996; Kvenvolden, 1993; Sloan and Koh, 2007; Claypool and Kaplan, 1974). On reflection seismic profiles, the phase boundary between methane hydrate and underlying free gas produces a prominent negative-polarity reflection known as a bottom simulating reflector (BSR) (Bale et al., 2014; Kinoshita et al., 2011; Holbrook et al., 1996). BSRs have been observed within the forearc basins of convergent plate margins worldwide, such as offshore Oregon (Petersen et al., 2007; Kumar et al., 2006; Milkov et al., 2003), South Shetland margin (Jin et al., 2003; Lodolo et al., 2002; Tinivella and Accaino, 2000), the Nankai Trough (Bale et al., 2014; Jia et al., 2016; Chhun et al., 2018; Kinoshita et al., 2011) and off southwest Taiwan (Lin et al., 2009; Chi et al., 2006; Chow et al., 2000; Schnürle et al., 1999), and are also observed in the Sanriku-Oki forearc basin in northeast Japan (Fig. 1). The existence of BSRs is often considered in terms of *in situ* gas generation (e.g., Paull et al., 1994), but could also indicate gas migration from deep successions (e.g., Haacke et al., 2007). Knowledge of the subsurface distribution of gas hydrate and free gas is important not only for evaluation of potential hydrocarbon gas resources but also for identification of potential geologic hazards associated with subsurface gas, such as submarine landslides (Kvenvolden, 1993; Sloan and Koh, 2007; Sun et al., 2017), and to understanding the role of gas hydrates in global climate change (Judd et al., 2002; Holbrook et al., 1996; Kennett et al., 2003; Paull et al., 1991).

The migration and accumulation of gas is often associated with tectonic activity (e.g., faulting and slumping) on plate convergent margins (e.g., Chhun et al., 2018). Several studies have characterized

* Corresponding author. Department of Earth Resources Engineering, Kyushu University, 744 Motooka Nishi-ku, Fukuoka 819-0395, Japan.
E-mail addresses: chandoeun.eng@mine.kyushu-u.ac.jp (C. Eng), tsuji@mine.kyushu-u.ac.jp (T. Tsuji).

https://doi.org/10.1016/j.marpetgeo.2018.10.013
Received 10 April 2018; Received in revised form 27 September 2018; Accepted 10 October 2018
Available online 12 October 2018
0264-8172/

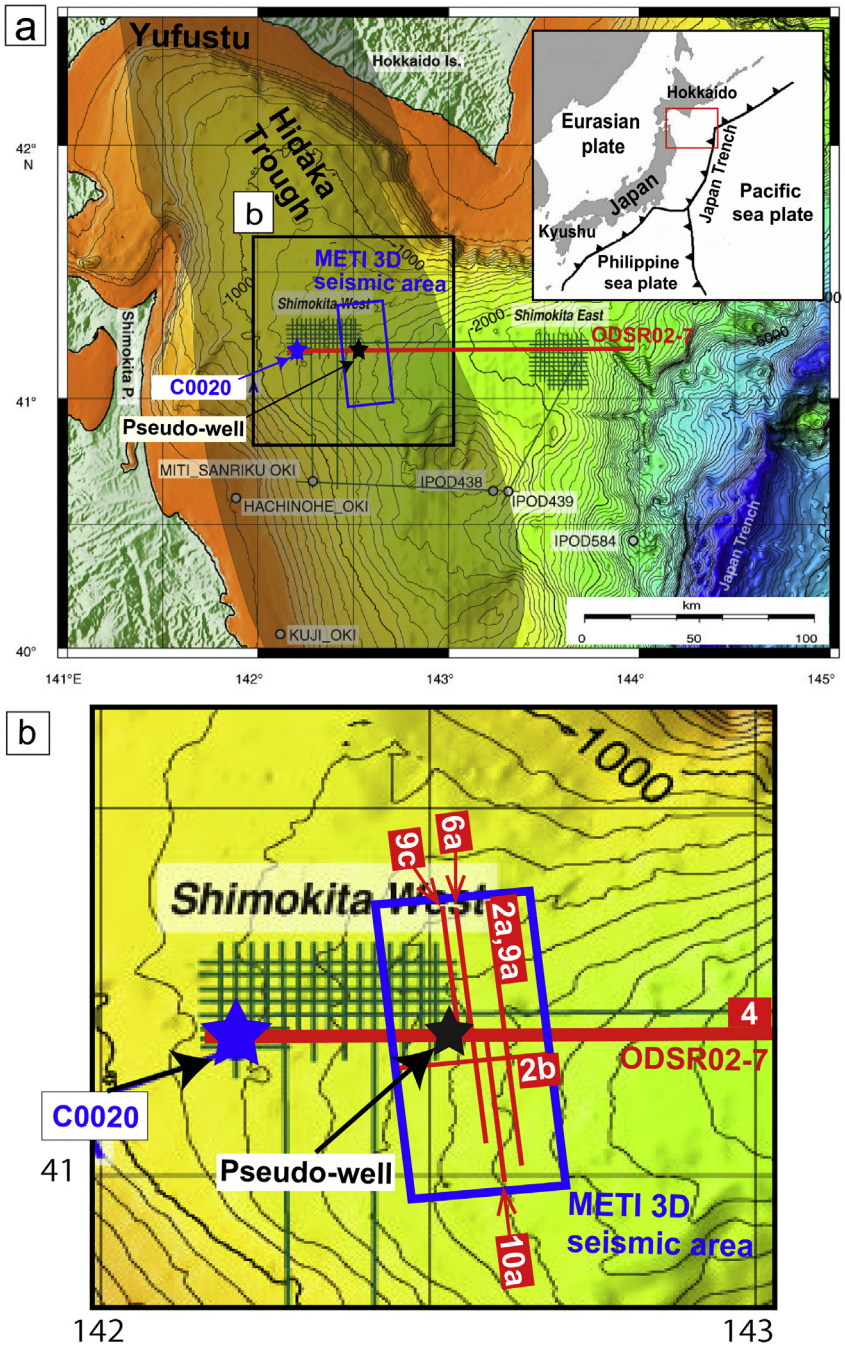

Fig. 1. (a) Location map of the study area offshore northeast Japan, with bathymetry (Inagaki et al., 2012). Inset map exhibits plate configuration around the Japanese Island and the location of the study area (red square). Grey shaded area indicates a continuation of the forearc basin parallel to the Japan Trench. (b) Enlarged bathymetry map around the METI 3D seismic survey area. Blue and black stars indicate the locations of Site C0020 and a pseudo-well (see text). Blue rectangle indicates the METI 3D seismic volume. Thin red lines within the blue rectangle are the locations of seismic profiles displayed in this paper, with figure numbers. Thick red lines in panels (a) and (b) indicate 2D seismic line ODSR02-7. (For interpretation of the references to color in this figure legend, the reader is referred to the Web version of this article.)

hydrocarbon gases migrating through faults, from biogenic and deep thermogenic sources, to accumulate in shallow reservoirs (Cartwright, 2007; Jia et al., 2016; Crutchley et al., 2015; Sun et al., 2012a,b; Tsuji et al., 2015; Ijiri et al., 2018). Other studies have shown the influence of slump deposits on hydrocarbon migration and trapping. Slumps may form consolidated layers that act as seals to fluid flow (Sun et al., 2017; Dugan, 2012; Gong et al., 2014; Guan et al., 2016), but may also act as preferential pathways for focused fluid flows (Guan et al., 2016; Gamboa and Alves., 2015; Gamboa et al., 2011; Riboulot et al., 2013). Slumps may also serve as reservoirs for free gas and gas hydrate (Sun et al., 2012a,b; Alves et al., 2014). These studies show that the role of slump deposits on gas migration and accumulation remains to be clarified.

The Sanriku-Oki forearc basin located on the Japan Trench is a likely southern extension of the Yufutsu oil and gas field on the southern coast of Hokkaido (Fig. 1; Osawa et al., 2002; Oda, 2003). In the Sanriku-Oki forearc basin, many slumps are observed on seismic data (Morita et al., 2012), accumulated in a context of tectonic subsidence (Von Huene and Lallemand, 1990) and large earthquakes along the plate interface (e.g., the 2011 Mw9 Tohoku-oki earthquake; Tsuji et al., 2013). BSRs are also observed, along with strong reflections immediately below them (Fig. 2) that suggest the presence of methane gas due to a strong upward flux of free gases from deep hydrocarbon sources (Bale et al., 2014; Taira et al., 2015; Inagaki et al., 2012). Gas accumulations give rise to acoustic impedance contrasts that produce strong reflections and are of opposite polarity to the sea floor reflection (Berndt et al., 2002; Judd and Hovland, 1992; Andreassen et al., 2007; Jia et al., 2016). Analyses of logging data and core samples from Integrated Ocean Drilling Program (IODP) Site C0020 identified coal beds 0.3–7.3 m thick in formations at depths of ~1.5–2.5 km below the seafloor (Figs. 1 and 3; Inagaki et al., 2012). These coal beds are the likely source of gas in the Sanriku-Oki forearc basin (Oda, 2003; Osawa

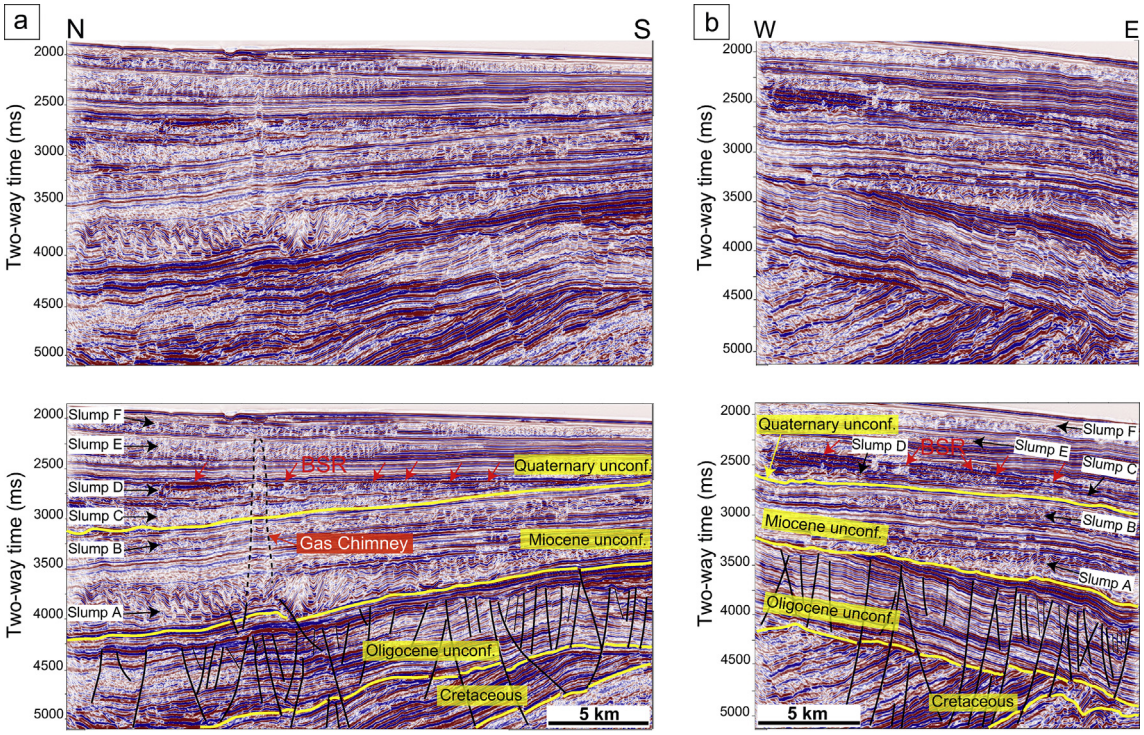

Fig. 2. Seismic reflection profiles extracted from the METI 3D seismic volume across the Sanriku-Oki forearc basin with and without interpretation, in (a) N–S direction and (b) E–W direction. The strong reflection from 2500 to 2600 ms two-way traveltime indicates the bottom-simulating reflection or BSR (red arrows). Yellow lines represent unconformities (Cretaceous, Oligocene, Miocene and Quaternary), dated by correlation of our seismic data with seismic stratigraphy from Takano (2017). Black lines indicate major normal faults. Gas chimney delimited by black dashed line. Black arrows indicate interpreted slump deposits (A to F). (For interpretation of the references to color in this figure legend, the reader is referred to the Web version of this article.)

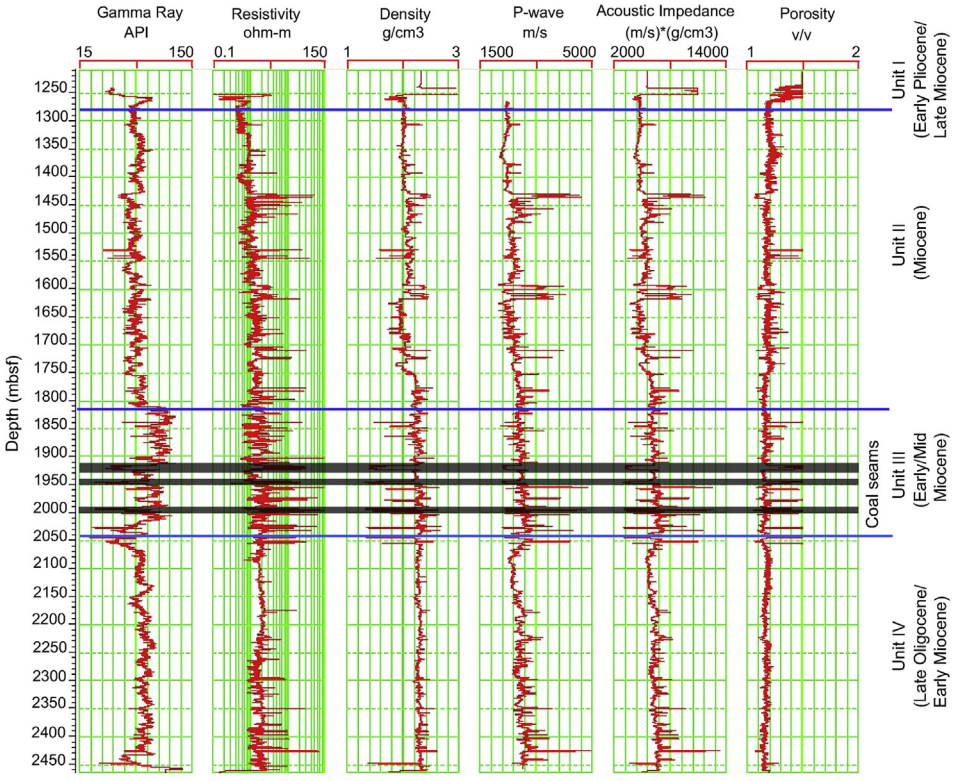

Fig. 3. Downhole log data from 1200 to 2466 m below seafloor (mbsf) at IODP Site C0020, showing natural gamma ray, resistivity, density, porosity, P-wave velocity, and acoustic impedance (Inagaki et al., 2012). Coal-bearing intervals including several coal seams are marked by black color. Blue lines are the boundaries of four lithological units and their ages. (For interpretation of the references to color in this figure legend, the reader is referred to the Web version of this article.)

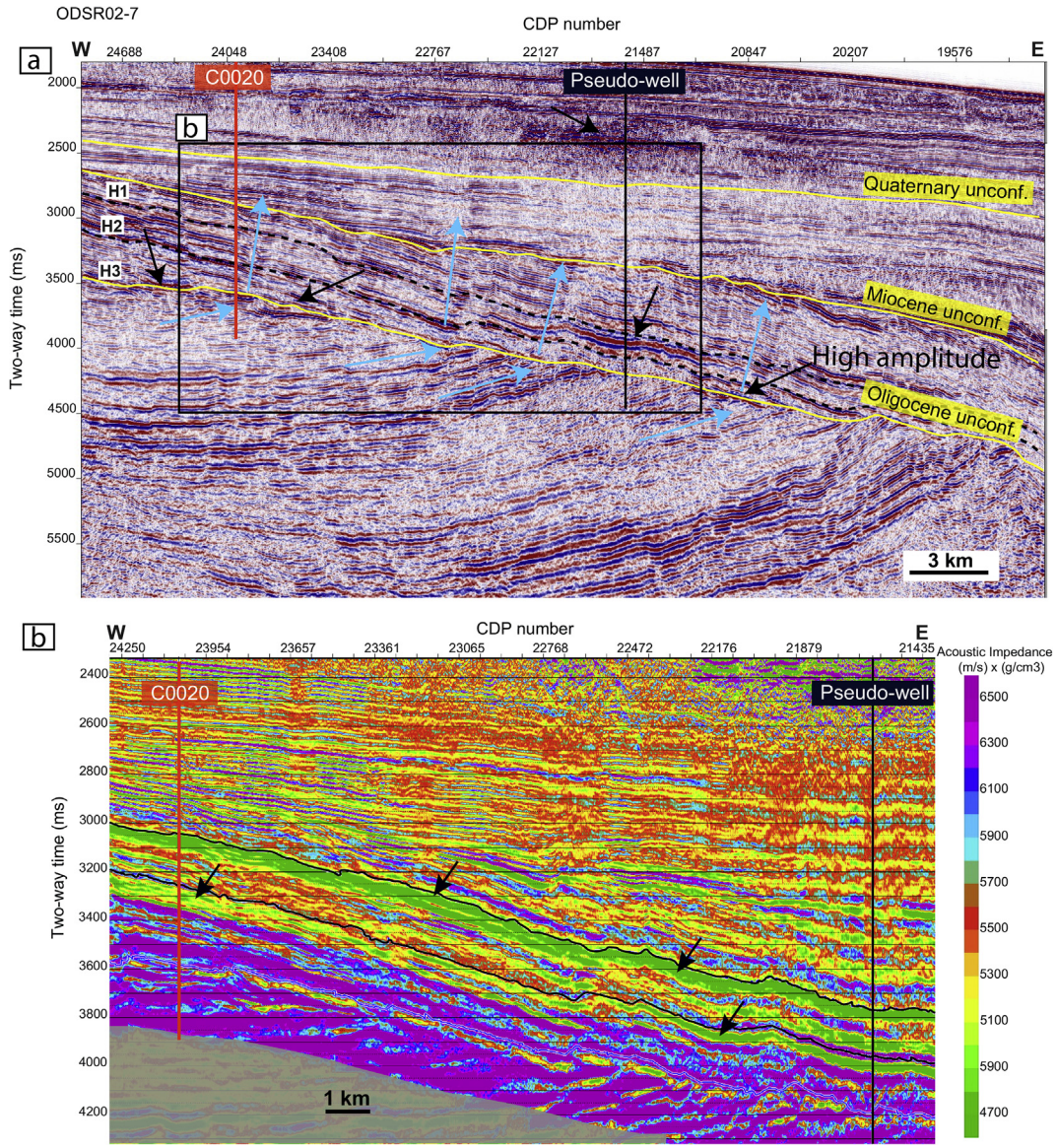

Fig. 4. (a) 2D seismic reflection profile ODSR02-7. Blue arrows indicate interpreted fluid migrated pathway through porous formations and faults. Black arrows indicate high amplitude reflection interpreted as gas-bearing sediments. Yellow lines indicate unconformities (Oligocene, Miocene, and Quaternary). These unconformities are produced by correlation of our seismic data with seismic stratigraphy from Takano (2017). Black rectangle refers to the acoustic impedance profile displayed in panel (b). (b) Acoustic impedance of 2D seismic profile ODSR02-7. Vertical red and black lines indicate IODP Site C0020 and pseudo-well generated at CDP 21610, respectively. Black arrows indicate intervals of low acoustic impedance that are interpreted as coal-bearing interval. (For interpretation of the references to color in this figure legend, the reader is referred to the Web version of this article.)

et al., 2002; Inagaki et al., 2016). The many studies of the Sanriku-Oki forearc basin have included investigations of its hydrocarbon potential (Osawa et al., 2002), stratigraphy and seismic facies (Takano and Tsuji, 2017), tectonic evolution (Von Huene and Lallemand, 1990, Itoh and Tsuru, 2006; Regalla et al., 2013; Takano et al., 2013), and potential for coal exploration (Inagaki et al., 2016; Gross et al., 2015). However, the relationship between hydrocarbon systems, tectonic activity and sediment instability in the Sanriku-Oki forearc basin has not been well revealed.

In this study, we use seismic attribute analyses of 3D seismic data to estimate the spatial distribution of coal-bearing strata (i.e., potential source), gas-bearing sediments (i.e., reservoir), faults, slump deposits and gas chimneys (i.e., migration pathways). These spatial distributions allow an improved understanding of the geological structures and tectonic events that controlled hydrocarbon system. In particular, seismic attribute analyses enable us to model a relationship between faults, slumps and gas migration. We further clarify the role of sediment instability in subduction zones in influencing the migration and accumulation of gas hydrate and free gas.

2. Geological setting and basin evolution

The Sanriku-Oki forearc basin lies between the northeastern Japan Arc and the Japan Trench within a narrow N–S trending zone extending from the southern coast of central Hokkaido to the area offshore the northeast coast of Honshu Island (Fig. 1). The forearc basin was formed as a consequence of subduction of the Pacific plate beneath the northeastern Japan Arc (Maruyama et al., 1997; Gross et al., 2015). The Sanriku-Oki basin is expected to contain similar hydrocarbon reserves to those of the Yufutsu oil and gas field on the southern coast of Hokkaido (Osawa et al., 2002; Oda, 2003; see black shaded area in Fig. 1a), because these oil and gas fields show significant volumes of hydrocarbon sources from Cretaceous and Oligocene coals and coaly shales.

The forearc basin is bordered to the east by an area uplifted along

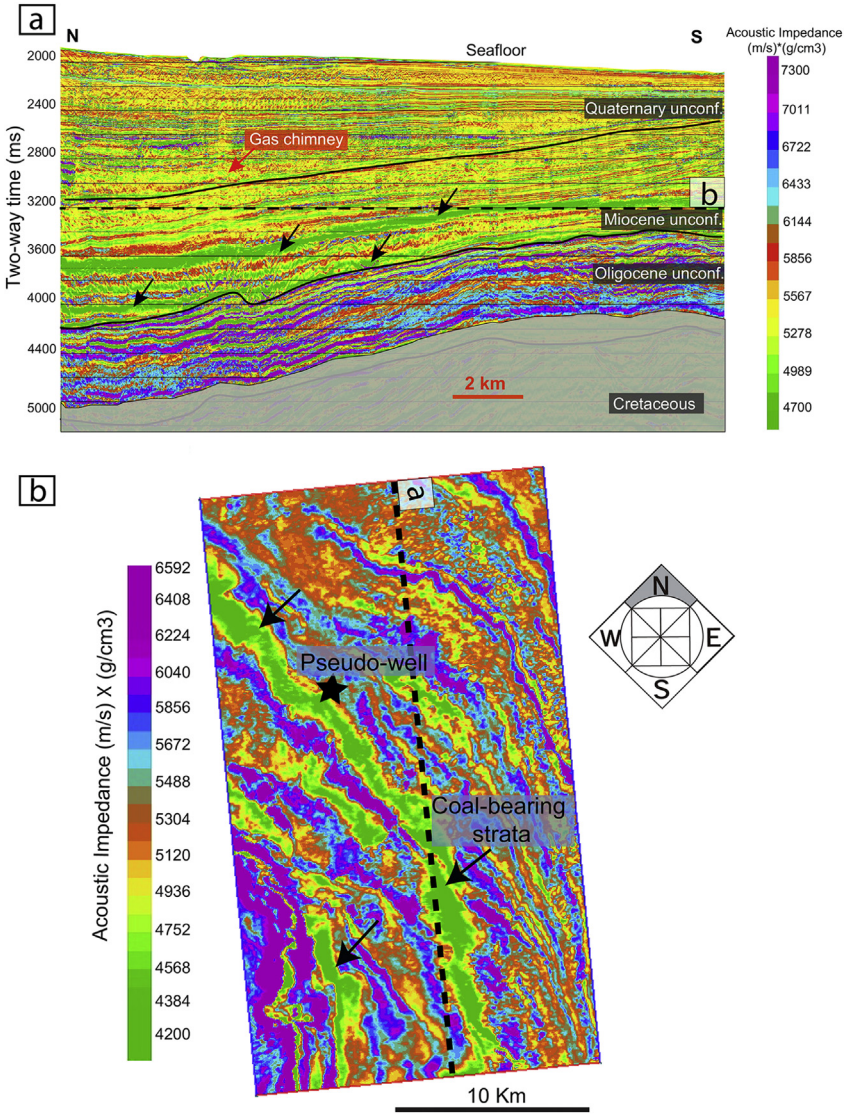

Fig. 5. (a) Acoustic impedance along a profile from the METI 3D seismic volume. Black lines indicate unconformities. (b) Time-slice of acoustic impedance volume at 3.2 s two-way travel time TWT (black dashed line in panel (a)). Black arrows indicate low acoustic impedance interpreted as coal-bearing intervals. Black star shows the location of pseudo-well. Black dashed line in panel (b) is the location of acoustic impedance profile of panel (a).

the trench slope break (Gross et al., 2015). Infilling of forearc basins began in the Late Jurassic and has continued until the present to produce a thick succession (~6000 m) comprising several stratigraphic packages separated by four major unconformities (Cretaceous, Oligocene, Miocene, and Quaternary) (Fig. 2; Takano and Tsuji, 2017). The depositional environment during the Cretaceous and Paleogene was predominantly fluvial and included deposition of coals and coaly shales. The vitrinite reflectance of the coals varies from 0.5 to 0.7% (Osawa et al., 2002), typical of relatively immature to mature coals. *In situ* temperatures derived from the thermal gradient (~22.5 °C/km) are well within the habitable range of microbes. The high total organic carbon content and its type (II/III) indicate that coals succeeded in producing natural gas (Osawa et al., 2002; Oda, 2003). During Late Paleogene, the main source of sediment was the volcanic arc in the west side of the forearc basin (Von Huene et al., 1982). During the Late Oligocene and Miocene, the depositional environment of the basin began to change to a slope environment in response to broad-scale subsidence along a hinge line (Takano, 2017). As a consequence, the Oligocene unconformity was overlain by a transgressive succession, in turn overlain by a deep marine muddy facies that comprises the Neogene and Quaternary succession.

3. Data and methods

3.1. Downhole data

The Integrated Ocean Drilling Program (IODP) drilled Site C0020 in 1180 m water depth (blue star in Fig. 1) within the 2D seismic survey area in 2012 (Inagaki et al., 2012). Site C0020 is the extension of JAMSTEC hole C9001 drilled during a *Chikyu* shakedown cruise in 2006. In hole C9001, drilling by both riserless and riser drilling systems terminated at 647 m below the sea floor (mbsf). IODP Expedition 337 drilled from 647 mbsf to the final depth of 2466 mbsf. The logging data used here is from 1252 to 2466 mbsf, and includes gamma ray, resistivity, sonic velocity, density, and combination nuclear magnetic resonance porosity (Fig. 3). Sonic velocity and density are used herein for acoustic impedance (AI) inversions of seismic data.

Coal seams were identified based on comparison of log data with lithology described from core samples, and can be correlated with the available seismic data. Fourteen coal layers were found at depth between 1825 and 2450 mbsf (Fig. 3; Inagaki et al., 2016). Coal-bearing intervals consist of coal, coaly shale, sandstone, siltstone, beach sand, carbonates and conglomerates coal-bearing intervals predominate in

Unit III (Fig. 3) at IODP Site C0020; at depths corresponding to coal-bearing intervals, P-wave velocities, densities, and gamma ray decrease sharply, and resistivity increases.

3.2. Seismic data

In 2002, 2003, a 2D seismic survey off Shimokita Peninsula was carried out by the Japan Agency for Marine-Earth Science and Technology (JAMSTEC) using the *R/V* Polar Duke and *R/V* Polar Princess. The survey covered a 15 km (N–S) × 30 km (E–W) area with line spacing of about 2 km (Fig. 1; Inagaki et al., 2012). Acquisition involved a source array of 3500 in^3 at 6 m depth, and a single streamer with 408 primary and 12 auxiliary channels totalling 5100 m in length and towed at 10 m depth (Taira et al., 2015). Processing of the 2D data involved the following procedures: bandpass filtering, migration, multiple removal with parabolic radon transform and deconvolution (Fig. 4a).

In 2008, a 3D seismic survey was conducted by the Ministry of Economy, Trade and Industry Japan (METI) using the 3D seismic vessel, *R/V Shigen* (Figs. 1 and 2). The METI 3D seismic data was acquired by the National Program for Oil and Gas Prospecting (2010 FY Geophysical Survey and Basin Evaluation Project "Sanriku-Oki 3D"). The 3D survey covers an area of 806.3 km^2. The inline direction of the METI 3D seismic survey is oriented 7° to the west. The dimensions of the survey area are 40 km for in-line (N–S) direction and 20 km for cross-line (W–E) direction. The bin size is 12.5 m for the inline direction and 25.0 m for the crossline direction. Acquisition was implemented using a source array of 3090 in^3 at 6 m depth, and the source characteristics are similar to the 2D seismic data (ODSR02-07). The length of streamers is ~5000 m. The data processing included bandpass filter, surface related multiple elimination (SRME), radon demultiple, and pre-stack time migration (PSTM).

3.3. Seismic attributes

Seismic images generated using seismic attribute volumes enhance or quantify certain anomalies or characteristic features, which are unrecognizable on the original amplitude data (Taner et al., 1979). To investigate hydrocarbon systems in Sanriku-Oki forearc basin, we used a series of seismic attributes, such as acoustic impedance, envelope, chaos, ant-tracking, and dip illumination (Figs. 4–8). We performed acoustic impedance inversion to characterize the coal-bearing strata, because the strata can be characterized as low acoustic impedance in logging data. Faults were identified using chaos and ant-tracking map. We calculated the envelope attribute (i.e., reflection strength) to enhance gas-bearing sediments. We further used the dip illumination attribute to characterize slump deposits (e.g., strike and dip of imbricate structures).

3.3.1. Acoustic impedance inversion

The inversion process involves calculating a subsurface acoustic impedance model consistent with corresponding seismic data (Ecker et al., 2000; Lu and McMechan, 2002; Jia et al., 2016). We used acoustic impedance inversion to spatially extend the high-resolution geologic information available from well data.

Acoustic impedance *AI* is the product of rock density ρ and *P*-wave velocity V_p.

$$AI = \rho \times V_p \tag{1}$$

The reflection coefficient r_i can be calculated from the acoustic impedance contrast at formation interface, as follows:

$$r_i = \frac{AI_{i+1} - AI_i}{AI_{i+1} + AI_i} \tag{2}$$

where AI_i is the acoustic impedance of the overlying formation, and AI_{i+1} is the acoustic impedance of underlying formation. The seismic trace can be considered as a convolutional result from the reflectivity r_i and the source wavelet W_i.

$$T_i = \sum_j r_j W_{i-j+1} + e_i \tag{3}$$

where T_i is seismic response (i.e., recorded seismic traces), and e_i represents additive measurement noise. To estimate acoustic impedance from the post-stack reflection waveforms, we used inversion based on the convolution model. The seismic inversion procedure employed in this study involves horizontal picking, wavelet extraction, log to seismic traces calibration, estimation of low-frequency model and seismic inversion using simulated annealing (Maver and Rasmussen, 1995; Husse and Feary, 2005).

In this study, one well (C0020) is present within the area covered by the 2D seismic profile and no well has been drilled within the METI 3D seismic survey area (Fig. 1). Therefore, pseudo-well data was extracted from the acoustic impedance results of a 2D seismic line at its intersection with 3D seismic volume (CDP 21610 of 2D seismic line ODSR02-7; see Figs. 1 and 4b), and was used for inversion of the 3D seismic data. This allowed us to tie the acoustic impedance data from IODP Site C0020 along the 2D seismic line (ODSR02-7; Fig. 4) into the METI 3D seismic volume (Fig. 5). In this approach using a pseudo-well, different source characteristics (e.g., frequency component) could generate error in inversion results. However, because of the similar source characteristics of the 2D and 3D seismic data used in this study, these errors could be limited. Using this pseudo-well information with the METI 3D seismic data, we generated a 3D acoustic impedance model of coal-bearing intervals (Fig. 5).

3.3.2. Envelope attribute

Envelope attribute or reflection strength can be computed as a modulus of complex trace, and thus is independent of the phase or polarity of the seismic data, both of which affect the apparent brightness of a reflection (Taner et al., 1979). This attribute is useful in detecting bright spots caused by gas accumulations and detecting major lithological changes caused by strong energy reflections and sequence boundaries (Fig. 6; e.g., Tsuji et al., 2012).

3.3.3. Chaos and ant-tracking attributes

Chaos attribute is a measure of the lack of organization in the dip and azimuth estimates (Pigott et al., 2013; Koson et al., 2014) and can be used to evidence faults and discontinuities (Fig. 8a). Zones of maximum chaos value indicate discontinuities such as faults, fractures, and angular unconformities, while zones of minimum chaos value correspond to bed continuity (Koson et al., 2014; Pigott et al., 2013). In this study, we used the chaos attribute as input to employ the ant-tracking attribute (Fig. 7b).

Ant-tracking is an algorithm that extracts continuous features to facilitate fault identification. This attribute is an extension to the heuristic 'ant system' algorithm developed from observations of ant colonies (Dorigo et al., 1996). The method uses the principles of swarm intelligence to find and enhance fault structure from spatial discontinuity. This approach has several parameters, such as initial ant boundary, ant-track-derivation, ant-step size, and stope criteria. In this study, several different parameters were tested and the optimum parameters chosen. After applying seismic conditioning (structural smoothing) to reduce noise and enhance spatial discontinuities via chaos, we generated an ant-tracking volume (fault surface extraction).

3.3.4. Dip illumination attribute

To calculate the dip illumination attribute, we used a 5 × 5 neighborhood of traces for dip scan (Aqrawi et al., 2012). The combination of dip scan with an Euler directional component is able to highlight dip magnitude, directional dip, and remove noise embedded in the seismic data. This attribute is a good indicator of geological structures, such as discontinuities (faults) and chaotic intervals (slumps). In our 3D seismic

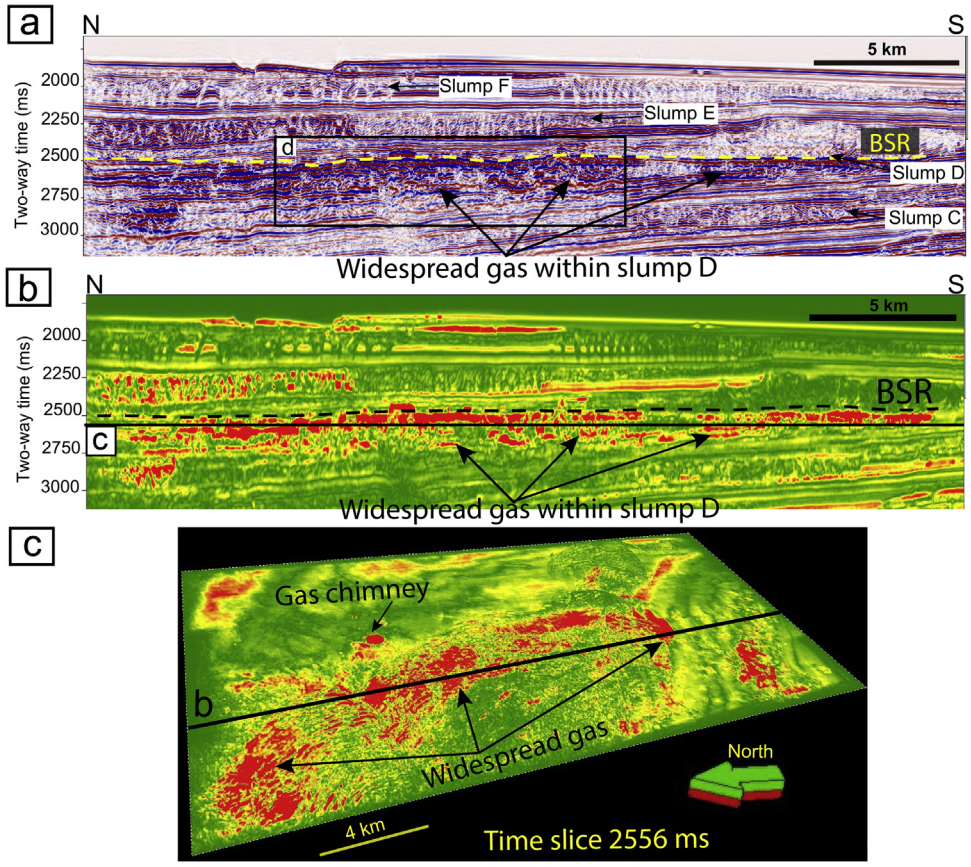

Fig. 6. (a) Seismic profile from the METI 3D seismic volume in a N–S direction. Yellow dashed line indicates BSR. Black arrows indicate high amplitudes interpreted as free gas. Black rectangle refers to the P-wave velocity profile displayed in panel (d). (b) Envelope attribute emphasizing spatial gas distribution. Black dashed line and arrows indicate widespread BSR and free gas zone below BSR, respectively. Black line indicates time slice beneath BSR, which shows in panel (c). (c) Time-slice (at 2556 ms TWT) of 3D envelope volume showing free gas-bearing sediments. (d) High-resolution P-wave velocity illustrating gas hydrate (high velocity above BSR) and free gas accumulation (low velocity beneath BSR) within slump interval (Kret et al., 2018). Black dashed line indicates BSR. (For interpretation of the references to color in this figure legend, the reader is referred to the Web version of this article.)

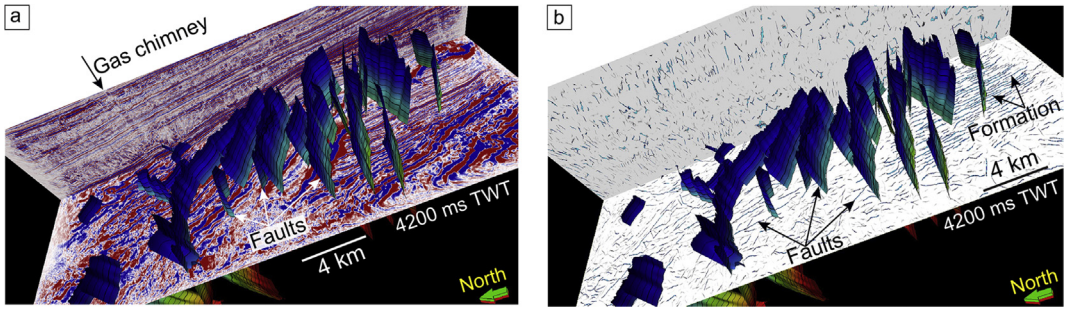

Fig. 7. (a) 3D geometry of normal faults beneath the Miocene unconformity extracted from the METI 3D seismic volume. In this figure, N–S seismic reflection profile and time-slice at 4200 ms TWT are also displayed. (b) 3D geometry of normal faults on the ant-tracking volume. The faults are enhanced by the ant-tracking attribute.

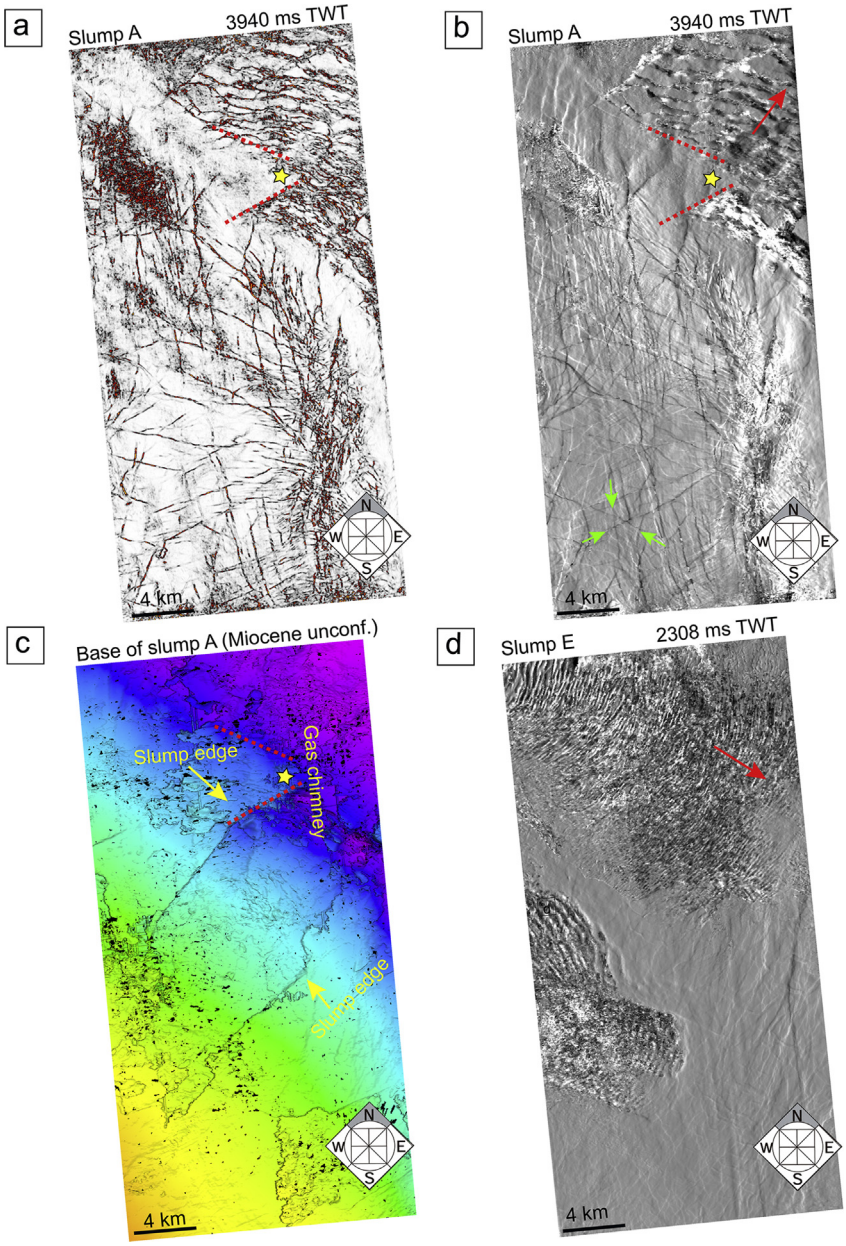

Fig. 8. Plan-view (time-slice) extracts of attributes from the METI 3D seismic volume: (a) Chaos attribute at 3940 ms TWT showing edges of slump A in the north-eastern part of the survey area and faults. Yellow star indicates location of chimney, and red dashed lines are slump edges beneath the gas chimney. (b) Dip illumination attribute at 3940 ms TWT showing slump A. Red arrows show the slump flow direction. Green arrows indicate normal faults whose strikes are NW–SE, NE–SW and N–S. (c) 3D geometry of base of slump A (or Miocene unconformity) showing slumping edges. Color shows TWT, and colder color indicates deeper. (d) Dip illumination attribute at 2308 ms TWT showing slump E. Flow direction of slump E (red arrow) is different from those of other slumps. (For interpretation of the references to color in this figure legend, the reader is referred to the Web version of this article.)

data, this seismic attribute was useful to characterize the slumps and their imbrication features (Fig. 8b and d).

4. Results – seismic observations and interpretations

4.1. Coal-bearing strata as hydrocarbon sources

As the lateral distribution of coal-bearing strata in the Sanriku-Oki forearc basin cannot be determined from seismic reflection data alone, we used acoustic impedance data to achieve this objective (Figs. 4b and 5). An inverted acoustic impedance profile of part of east–west 2D seismic line ODSR02-7, crossing IODP Site C0020, shows two intervals characterized by lower acoustic impedance, which we interpreted to represent coal-bearing strata interbedded with clastic sediments (Fig. 4b). They appear to be continuous in the time window from 3.0 to 3.4 s two-way traveltime (TWT). Furthermore, we investigated the distribution of coal-bearing strata in the METI 3D seismic volume by using a horizontal time slice at 3.2 s TWT (Fig. 5b). The coal-bearing strata appear as bands of relatively low acoustic impedance of ~4200–5200 (m/s × g/cm^3) within the time slice. The acoustic impedance values are consistent with sonic and density log data for coal seams penetrated at IODP Site C0020 (Fig. 3).

Although Inagaki et al. (2016) identified several coal seams in Unit III (Fig. 3), we could identify only two coal-bearing strata in our acoustic impedance volume (green in Figs. 4b and 5) thick enough to be resolved by the low-frequency seismic data. The acoustic impedance data for these two major coal-bearing strata (Fig. 5b) indicate only small lateral variations of thickness, which suggests that they may extend continuously across the forearc basins in similar thickness (Oda, 2003; Koide and Kuniyasu, 2006; Osawa et al., 2002). In IODP Site C0020, these coal-bearing intervals correspond to lower acoustic impedance than the overlying and underlying fine-grained clastic sediments (shales, siltstones, and shaly sandstones) recognized by Inagaki et al. (2016) and Glombitza et al. (2016). Because the structure of coal-bearing intervals could be similar in our study area including 3D and 2D seismic area, the continuity of the low acoustic impedance bands can be used to map the major coal dominant strata within the entire 3D seismic volume.

The coals in Unit III (Fig. 3) were deposited in tidal flats, channels, wetlands, and fluvial environments (back marshes and swamps) during the Late Oligocene to Early Miocene. Subsequent subsidence of the forearc basin led to the deposition of a thick overlying sequence of deep marine sediments (Taira et al., 2015; Oda, 2003; Noda et al., 2013; Inagaki et al., 2012; Takano, 2017). The total organic carbon content of the coals ranges from 9.9 to 40.9 wt% (Inagaki et al., 2013), which makes them excellent hydrocarbon source rocks (Peters and Cassa, 1994). The estimated maximum burial temperatures derived from vitrinite reflectance are 400–440 °C, indicating that the organic matter in the coals is in a thermally immature to early mature state for gas generation (Inagaki et al., 2013). The type II/III kerogens of these coals and their medium to high hydrogen index indicate that they are more likely to produce hydrocarbon gas than oil (Osawa et al., 2002; Oda, 2003), which is supported by the presence of methane and other hydrocarbon gases, as well as N_2, O_2, H_2, and CO, in the coal-bearing strata at Site C0020 (Inagaki et al., 2012).

Deeper Cretaceous to Paleogene (lower to middle Eocene) coal-bearing strata deposited in coastal bays to braided-fluvial environments are a potential alternative source rock for hydrocarbon gas in this area (Takano and Tsuji, 2017). Vitrinite reflectance and well log data from the nearby Sanriku-Oki well site (Fig. 1) indicate the presence of immature to mature coal beds in these deep strata (Osawa et al., 2002). Indeed, iodine concentrations and radioisotopic compositions of pore water from below the base of the gas hydrate layer at IODP Site C0020 show that the pore water is older than the host sediments, suggesting that the gas accumulations are the result of long-term migration from the deep biogenic sources (Tomaru et al., 2009). The drilling at Site C0020 did not reach these deeper strata. Because of the limited logging interval for acoustic impedance inversion, the Cretaceous to Paleogene coal-bearing strata cannot be identified by acoustic impedance results. Coal seams are common in the Cretaceous to Paleogene successions of the Sanriku-Oki forearc basin (Osawa et al., 2002; Inagaki et al., 2012). The forearc basin was characterized by Takano (2017) as a shelved and benched forearc basin in which uplift of the trench-slope break resulted in the emergence of a ridge along the eastern margin of the basin that provided a barrier to the open sea trenchward of the basin. Thus, the forearc basin was overfilled to produce an aggradational sequence of coal-bearing sediments. Based on their vitrinite reflectance values, these coal seams are thermally more mature than those deposited during the Oligocene and early Miocene (Coals in Unit III). Given their higher total organic carbon content (40–60%) and type of organic carbon II/III, the coals are considered to be potential source rocks for hydrocarbon gases (Osawa et al., 2002, Takano, 2017). Takano and Tsuji (2017) noted that the Cretaceous to Paleogene succession contains many paleo-channels and coal-bearing fluvial sediments, thus providing potential for both source and reservoir rocks.

We suggest that high-amplitude reflections on our seismic profiles from Cretaceous to Oligocene sediments (Figs. 2 and 4a) represent hydrocarbons entrapped within sandy paleo-channels. Moreover, we suggest that highly porous lithological boundaries and numerous normal faults in these formations have provided upward migration pathways for hydrocarbon gases generated in the deep Cretaceous to Paleogene sedimentary sequences (blue arrow in Fig. 4a), and their accumulation within the porous Quaternary slump deposits. Due to lack of dipping faults in shallower Miocene to Quaternary sedimentary sequences, the migration of hydrocarbon gases through slumps (i.e., along imbricate internal thrusts and slump edges) may also play an important role in this sedimentary interval (Figs. 9–11). As we discuss later, thrusts within slumps could facilitate upward fluid flow (Gamboa and Alves, 2015; Gamboa et al., 2011; Riboulot et al., 2013).

4.2. Fluid migration pathways

Hydrocarbon gases in the Sanriku-Oki forearc basin could migrate upward from biogenic sources (Inagaki et al., 2012) through favoured conduits (e.g., faults, chimneys, and slumps) to accumulate in Quaternary reservoirs. Here, we interpret three types of migration processes of hydrocarbon gases in the basin.

4.2.1. Normal faults

Our application of the ant-tracking algorithm to the part of the METI 3D seismic volume revealed a complex patterns of faults within the Cretaceous to Quaternary succession below gas accumulation zone (Fig. 7b). The dip illumination attribute also clarifies the fault geometry (Fig. 8b). Many steeply-dipping normal faults were identified within the Cretaceous to Oligocene sedimentary succession, consistent with those we interpreted on seismic reflection profiles (Fig. 2). The largest offset of these normal faults is ~100 m. On time slices, we can identify three orientations of normal faults, striking NW–SE, NE–SW, N–S, and dipping to NE, NW, and E, respectively (Green arrows in Fig. 8b). These normal faults can be characterized as conjugate fault system.

The normal faults are associated with the subsidence typical of forearc basins (Xie and Heller, 2009). The average rate of subsidence in the Sanriku-Oki forearc basin during the Late Oligocene and Early Miocene was ~100 m/Ma (Takano, 2017; Regalla et al., 2013) and may have been a consequence of abrasional basal erosion of upper plate material at the plate interface during subduction (Von Huene and Lallemand, 1990; Takano, 2017). The resulting dynamic changes in the geometry of the upper plate and the shallow part of the downgoing slab created the accommodation space required for forearc basin subsidence. Regalla et al. (2013) and Tsuji et al. (2013) proposed that subsidence was dynamically caused by the extension of the upper plate during the interplate earthquakes. Subsidence of the forearc basin could be also associated with the increasing rate of convergence of the two tectonic plates in response to eastward motion of Japan Arc that was initiated during opening of the Japan Sea (Regalla et al., 2013). Thus, it is likely that the above-mentioned extensional stress was the cause of the normal faulting in the Cretaceous to Oligocene successions in the forearc basin. Moreover, the results of ant-tracking (Fig. 7b) show the network of normal faults to be accompanied by many small-offset faults, which we were unable to recognize during manual interpretation of seismic profiles. These normal faults could function as fluid migration pathways as well as hydraulic boundaries (e.g., Jia et al., 2016).

4.2.2. Slump deposits

The METI 3D seismic volume revealed six relatively low-amplitude intervals characterized by imbricate faulting and chaotic slump deposits. Here we note six dominant slumps as A to F (see Figs. 2 and 9a), although several minor slumping events occurred between the dominant sequences (e.g., above the top of slump A in Fig. 9c). These slumps have a wide distribution in the north-eastern part of the study area (Figs. 2, 9a and 9b), particularly within the Miocene to Quaternary succession. We propose two scenarios for deposition of the slumps: (1) They formed in areas of normal faulting (slump A) and (2) they formed in fault-free successions (slump B to F).

In slump A, on N–S seismic profiles (Fig. 9a), the imbricate thrusts north of a gas chimney dip to the south, whereas those south of the chimney dip north. In three dimensions (Fig. 8b), the imbricate thrusts on the north-east side of the chimney dip to south-west, while those on the south-east side dip in the opposite direction (north-east). The overall flow direction of slump A is from SW to NE (Figs. 8b and 9b), suggesting subsidence of the NE side of our study area. We observe that the early Miocene slump A has both the greatest lateral extent and the greatest thickness among the six slumps identified (Fig. 9a). It is thicker at the northern end of the profile shown in Fig. 9a (3.6–4.1 s TWT; ~500 m thick) and thinner in the south (3.0–3.1 s TWT; ~100 m thick), with a lateral extent of ~25 km. The basal shear surface of slump A is clearly identified on seismic profiles (Fig. 9) as a discontinuous, moderate-amplitude reflector showing basal erosion scours; it also truncates normal faults in the underlying Cretaceous succession (Fig. 9a and c). Thus, these were likely an important control

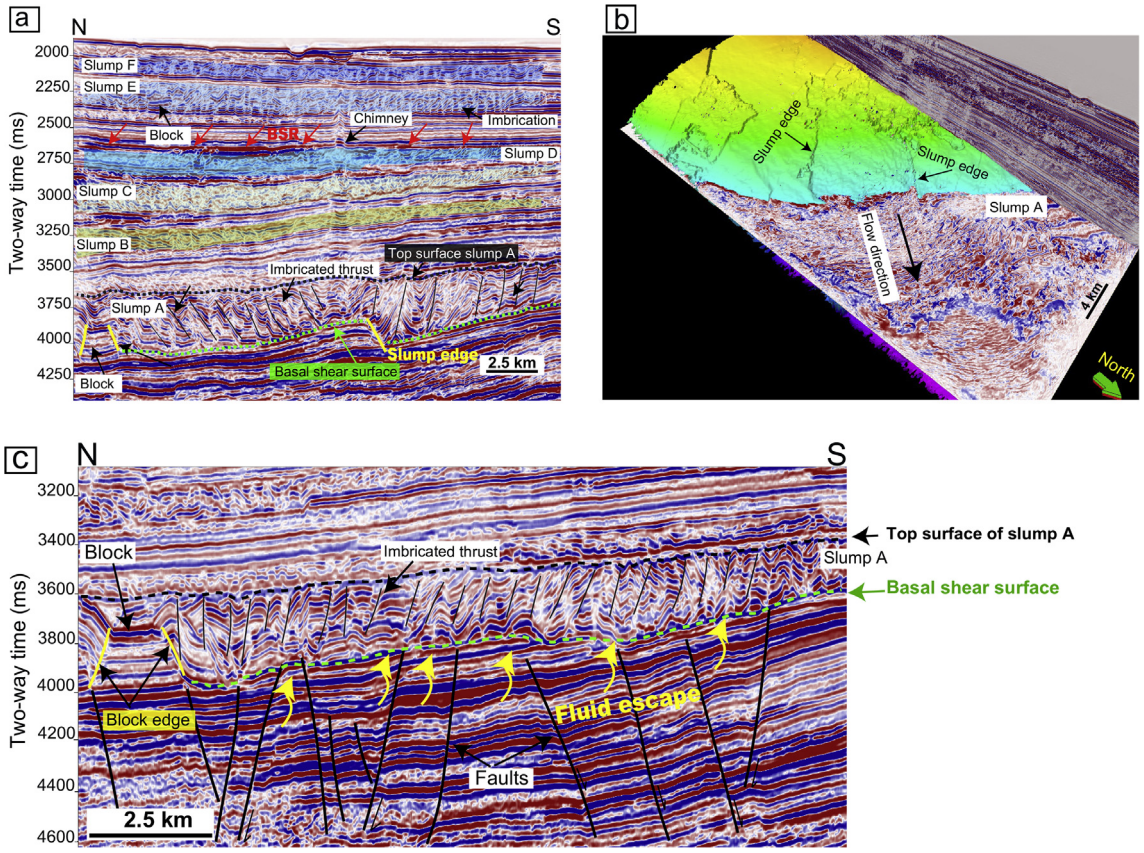

Fig. 9. Features of slumps observed on the METI 3D seismic reflection data: (a) Six main slump units are observed (A to F). Several slumps show internal imbrication and chaotic structures. Red arrows indicate the BSR. Black and green dashed lines indicate the top and basal surface of slump A, respectively. (b) 3D geometry of Miocene unconformity (base of slump A). The slump flow direction is SW to NE. (c) Enlarged seismic profile for slump A, seen to be developed above fault blocks (black lines). Yellow arrows indicate interpreted fluid escape routes from deeper levels, which may have induced slumping. Yellow lines indicate block edges. (For interpretation of the references to color in this figure legend, the reader is referred to the Web version of this article.)

on the development of slump A. Indeed, a step in the basal surface of slump A beneath the chimney is clearly controlled by two orientations of normal fault whose strikes are NE–SW and NW–SE (Fig. 8a, b, 8c, 9a, 10c). Activity on the normal faults probably generated the structural high in Cretaceous rocks underlying the gas chimney and could have triggered large-scale instability in younger strata (Fig. 9c). Because dips of imbricate thrusts within slump A are different across the step in the basal shear surface beneath the chimney (Fig. 9a), the step could be edge of two slumps. These seismic characteristics are similar to those attributed to mass-transport deposits associated with growth faulting in the Taranaki Basin, New Zealand (Panpichityota et al., 2018). Furthermore, as observed in other forearc basins (e.g., Lin et al., 2010; Lamarche et al., 2008), a Miocene subsidence event could have contributed to slope failure and gravitational deformation in the form of submarine slumping in the Sanriku-Oki basin, particularly slump A.

Slumps B to F appear to be restricted to the Late Miocene to Quaternary succession, shallower than the intervals in which faults occur, and lack clear imbricate faulting (Figs. 2 and 9a). Although we observe imbricate structures in some parts of the shallow slumps, the lateral spacing between the imbricate faults is much shorter than in slump A (Fig. 9a). The low reflection amplitude within these slumps indicates heterogeneous features and may indicate steep dips. Furthermore, the NW to SE flow direction of slump E (Fig. 8d) is different from that of other slumps (SW to NE; Fig. 8b). The difference in flow direction could indicate a change in subsidence patterns. High sedimentation rates in the Sanriku-Oki forearc basin from Cretaceous to Paleogene time may have resulted in overpressured fluids being trapped in the sediments (Flemings et al., 2008; Tsuji et al., 2008). High pore pressures may have created a pressure compartment (Morita et al., 2012; Kokusho, 2000), which caused the lubrication to enhance the slumping. Furthermore, high pore pressure could have contributed to the development of gas chimneys. Moreover, the Sanriku-Oki forearc basin is within a tectonically active region characterized by frequent large earthquakes (Tanioka and Sataka, 1996; Kanamori, 1971). Large earthquakes can instantaneously generate high pore pressures, even at large distances from the source fault (Nimiya et al., 2017). Such elevated pore pressures may have triggered slumping along low-dip sequence even if the area is far from the source fault. The oscillating ground motions of earthquakes can cause cyclic horizontal and vertical shear stresses, thereby increasing the gravitational force applied to sediments and leading to slumping (Leynaud et al., 2004; Strasser et al., 2007; Tsuji et al., 2017).

Slump D contains high amplitude reflectors beneath the BSR on seismic profiles (Fig. 6), suggesting that accumulation of gas may cause its anomalously high reflection strength (envelope value) within low-amplitude slump deposits. Kret et al. (2018) showed that the high reflection strength of slump D is due to low P-wave velocities as a result of the presence of gas as well as high pore pressures (Fig. 6d).

4.2.3. Gas chimneys

Gas chimneys record the vertical upward migration of fluids (Løseth et al., 2009; Cartwright, 2007; Gay et al., 2006). On seismic profiles from the METI 3D data volume (Figs. 2a and 9a), we interpret a vertically elongated feature in the Miocene to Quaternary succession, above the coal-bearing strata and the faulted block sequence, to represent a gas chimney. This feature occurs in the northeast part of our study area and is between ~2.4 and 3.6 s TWT (giving a height of ~1.2 km) and ~600 m wide. It cuts across horizontally stratified

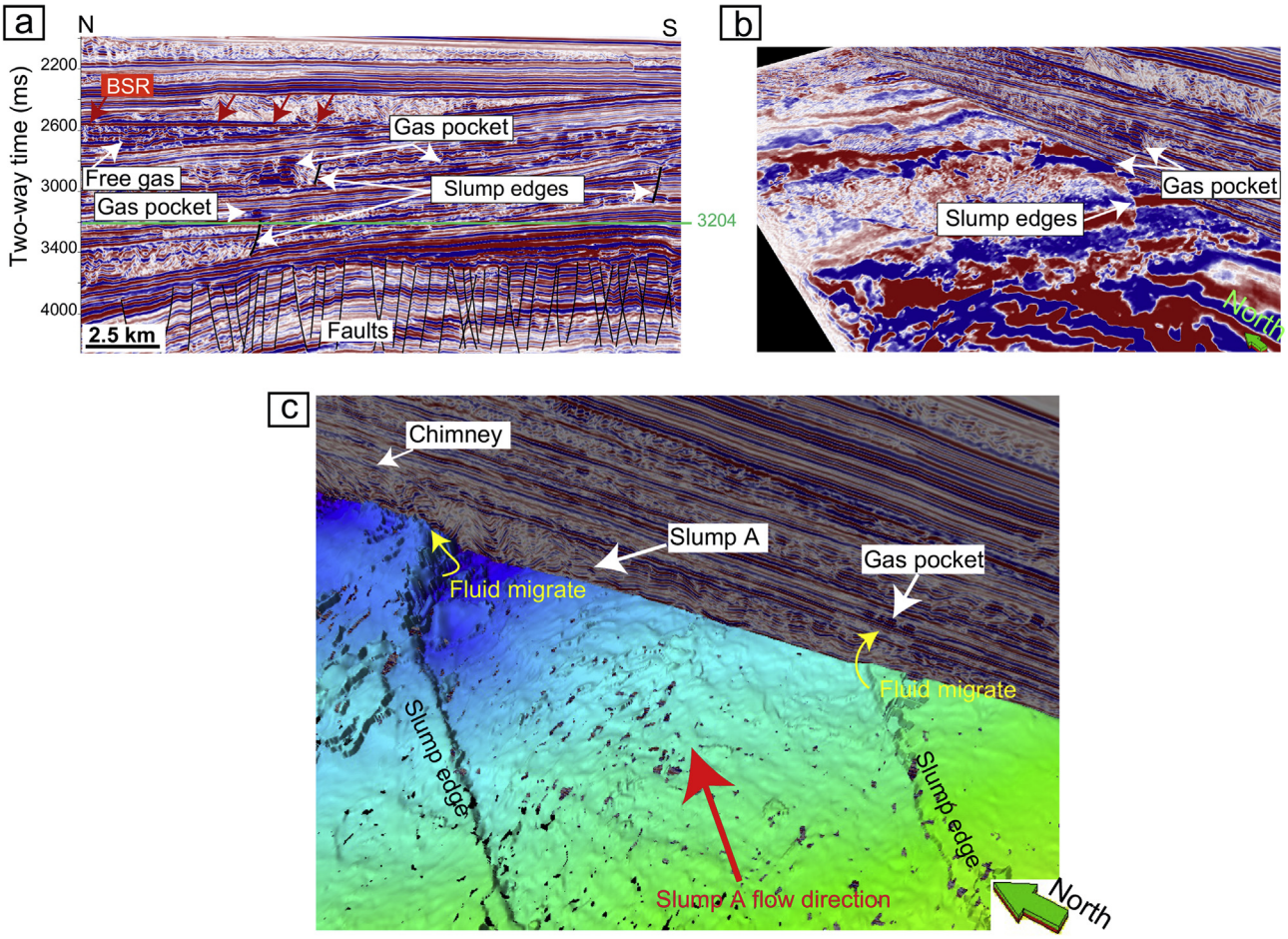

Fig. 10. Features of slump edges observed in the METI 3D seismic reflection data: (a) Seismic profile showing the relationship between gas pockets, slump edges, and fault blocks (black lines). Green line indicates the location of the time-slice beneath gas pocket shown in panel (b). (b) Time-slice at 3204 ms TWT depicting the interface of slump edges, and high-amplitude gas pockets. (c) 3D view of slump edges, gas pocket and chimney. Yellow arrows indicate interpreted fluid migration paths. (For interpretation of the references to color in this figure legend, the reader is referred to the Web version of this article.)

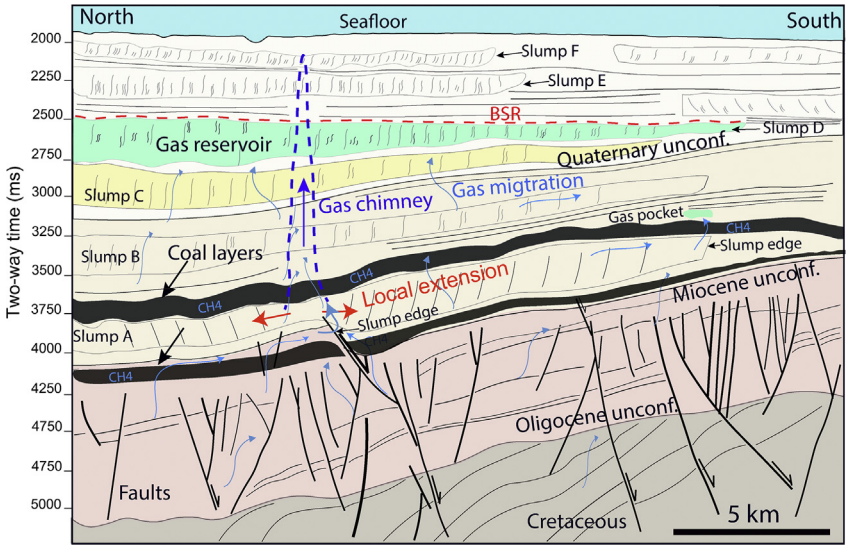

Fig. 11. Schematic diagram of pathways for hydrocarbon migration and accumulation relative to coal-bearing strata in Sanriku-Oki forearc basin (along a N–S profile).

reflections in the Miocene to Quaternary sequence and manifests as a narrow vertical zone of distorted seismic reflections (Fig. 2a).

The gas chimney in the Sanriku-Oki forearc basin has formed above potential source rocks (coal layers) and near the edges of slumps overlying the Miocene unconformity (Fig. 8a, b, 8c, 10c). We infer that fluid trapped beneath the low-permeable layers (green dashed line in Fig. 9a) migrated laterally in the up-dip direction and escaped upward from the boundary between layered sequence and the slump (i.e., slump edge) (Figs. 9 and 11).

4.3. Gas hydrate and free gas distribution

A high-amplitude but distinctly low continuity BSR, subparallel to and of opposite polarity to the seafloor reflector, was identified on seismic profiles in the Sanriku-Oki forearc basin (Figs. 2 and 6). The BSR exhibits all of the diagnostic characteristics of a seismic reflector at the base of the gas hydrate stability zone, or the top of a free-gas zone (Bale et al., 2014; Taira et al., 2015; Baba and Yamada, 2004; Hyndman and Spence, 1992; MacKay et al., 1994; Kvenvolden, 1998; López and Ojeda, 2006). The BSR is clearly observed within the Quaternary succession throughout the basin and appears to correspond with the top of Quaternary slump D (Fig. 2a), although it is disrupted by a gas chimney extending from the Miocene to the Quaternary unconformity.

The study area lies on the continental slope in water depths of around 1180 mbsf in a region where the geothermal gradient is 24 °C/km and the seafloor temperature is 3.6 °C (Inagaki et al., 2013; Tanikawa et al., 2016). These characteristics suggest that the subsurface environment lies within the methane hydrate stability zone (Kvenvolden, 1998). These conditions are similar to those of the methane hydrate stability zone in the Guajira basin offshore from Northern Colombia (López and Ojeda, 2006), the Kumano forearc basin in the Nankai Trough (Yamano et al., 1982; Chhun et al., 2018; Miyakawa et al., 2014), the Cascadia accretionary prism (Davis et al., 1990), and the Fiordland continental margin in New Zealand (Townend, 1997). In our study area, the spatial distribution of the BSR appears to be associated with the presence of gas chimneys, slump deposits (Fig. 9), and an underlying basement high (Figs. 2, 8, 9 and 11).

The particular seismic characteristics of sediments charged with free gas in the Sanriku-Oki forearc basin are high reflection amplitude anomalies (or high envelope value) (Fig. 6). These high-amplitude anomalies are visible in Quaternary-age slump D, which lies immediately below the BSR from 2.5 to 2.9 s TWT (~400 m depth range) and extends about 30 km N–S in the horizontal direction. Similar high-amplitude anomalies associated with gas-charged sediments have been observed in the South China Sea (e.g., Sun et al., 2012a,b) and in the Nankai Trough (e.g., Taladay et al., 2017; Tsuji et al., 2015; Kawabata et al., 2018).

Core samples from the Quaternary succession recovered at IODP Site C0020 are composed mainly of alternating beds of mud and sand with thin intercalations of volcanic tephra and locally developed gravel or sand layers (Inagaki et al., 2012). The Quaternary sand facies is a candidate reservoir rock for accumulations of natural gas. Core samples of slump deposits at Hidaka sedimentary basin (a northward continuation of Sanriku-Oki; Fig. 1) consist of sandy layers with dark olive clayey silt intercalations with porosity ranging from 52 to 72% (Noda et al., 2013), suggesting that porous slumps can be good reservoirs for hydrocarbons.

The overlying gas hydrate layer would provide an impermeable seal, preventing or inhibiting the escape of free gas and other fluids to the surface (Chhun et al., 2018; Gay et al., 2006) and promoting lateral up-dip gas migration through porous strata and gas accumulation in porous slump deposits beneath the BSR (Figs. 2, 6 and 9). The presence of sand and thrust-faults in slump deposits may represent an efficient system for fluid migration and the accumulation of free gas (Yu et al., 2014). Seismic profiles from the Sanriku-Oki forearc basin clearly show high-amplitude reflections, primarily within the slump D, which appear to be accumulations of free gas (Figs. 2 and 6). The acoustic impedance of the gas accumulation zone is lower and resulted in high amplitude reflectors overprinting the original slump structure (black arrows in Fig. 6a and b). Bangs et al. (1993) reported that even small amounts of free gas (1–2%) in sediments can cause anomalously high amplitude reflections.

5. Discussion – influence of tectonic activity on hydrocarbon migration

Our data provide evidence that tectonic activity in the convergent plate margin have influenced the migration pathways and accumulation of hydrocarbons. Our seismic data indicate more gas accumulations in the northeast of the study area (Figs. 6c and 10a). In response to subsidence during the Miocene, the Sanriku-Oki forearc basin transitioned from a shelved and benched type forearc basin to a slope type forearc basin (Takano, 2017; Takano et al., 2013), which suggests that the mud and sand facies deposited from both seaward and landward sources were thicker than those in southeast of the study area. The thick succession of Quaternary and Miocene sediments with a high proportion of porous slump deposits and sand facies in the northeast of the study area may also have contributed to the development of migration pathways and the trapping of hydrocarbon gases there, as demonstrated in the North Sea (Shanmugam et al., 1996). It is clear that faults, slumps and gas chimneys influence the migration of hydrocarbons in the northeast of the study area. The major faults there cut potential source rocks (i.e., coal beds) underlying the gas chimney (Figs. 2 and 11). In contrast, in the southeast of our study area, there is an abundance of steeply-dipping normal faults, but these faults do not cut potential source rocks (Figs. 2 and 11). Furthermore, there is an absence of chimneys and a lower frequency of slumps in the southeast part (Figs. 2 and 9) which perhaps provides an explanation for the limited migration and trapping of hydrocarbon gases within the Miocene to Quaternary interval.

The base of the gas chimney we observed is in Miocene strata at the edge of a slump, where slumping and faulting have caused intense deformation of the sediments (Figs. 10c and 11). Furthermore, the slump edges are controlled by deeper normal faults (Fig. 8b). The sequence directly beneath the gas chimney can accumulate hydrocarbons from surrounding strata because the slump edges are shallower than surrounding area (Figs. 2 and 11). This structural high is developed above the footwall of a major normal fault rooted in the basement. Local concentrations of hydrocarbons can increase fluid advection and initiate the development of a gas chimney (Løseth et al., 2009). The contrasting dips of thrusts in slump A on either side of the gas chimney (Figs. 9a and 11) suggest that the slump interval moved away from this position, and localized horizontal extension occurred in the succession beneath the chimney. Therefore, the higher vertical permeability along the faults and slump edges, and the localized extensional regime, allowed overpressured fluids to escape from deep Cretaceous biogenic sources through the chimney. Similar gas chimneys that cut across the slumps have been identified in the Hidaka trough, northern Japan (Noda et al., 2013).

The 3D seismic data provide evidence of gas pockets in the southeast part of our study area within the Miocene and Quaternary interval (Fig. 10). The gas pockets stand out as anomalously high amplitude reflections that occur locally within individual slumps and at slump edges. Slump edges are indicative of a local shear failure surface parallel to the slump flow direction (Bull et al., 2009), and extensional or compressional failures occur at the upslope and downslope limits of the slump (Fig. 10). They act as sharp boundaries between the porous slump interval and less permeable strata. Most of these slump edges are conspicuous on seismic sections (Figs. 9c and 10) and on time slices (Fig. 8a and b). In plan-view (Fig. 8c), the slump edges correspond to continuous planar features that represent likely fluid migration pathways. The internal structure of slumps, such as steeply-dipping surfaces

and imbricate faults (Figs. 8b, 9a and 9c), also provide potential routes for the percolation of fluids and their trapping in porous sediments. Because of the higher vertical permeability in slump deposits, hydrocarbon gases can propagate vertically through slumps or along their edges, and horizontally along sheared beds (Gamboa and Alves, 2015; Gamboa et al., 2011; Riboulot et al., 2013). Figs. 9b and 10c illustrate distinctive northern and southern slump edges, both of which may have provided conduits for migration of hydrocarbon gases. Thus, we suggest that slump deposits (i.e., products of sediment failure) provided an important control for the accumulation of gas reservoirs and gas pockets in the Sanriku-Oki forearc basin.

6. Conclusions

We used an analysis of 3D seismic attributes to identify potential hydrocarbon sources, migration pathways and accumulation processes in the Sanriku-Oki forearc basin. The insights derived from this study are of interest to understanding the nature of fluid migration within sedimentary basins, and are also relevant to gas exploration in the forearc basin. Our main findings are:

- Acoustic impedance calculated from 3D seismic data showed that coal-bearing intervals are widely distributed in the Late Oligocene to Early Miocene succession. We interpret these to be potential source rocks for hydrocarbon gases.
- Free gas is widespread in porous slumps of Quaternary age below a well-developed BSR. Several gas pockets were spatially associated with the edges of slump deposits. The largest gas accumulations are in the northeast of study area where the most intense slumping and faulting are observed, together with a gas chimney.
- A complex system of normal faults that cut Cretaceous to Miocene strata provide migration pathways for hydrocarbon gases from deep Cretaceous–Paleogene source rocks to Miocene strata. The normal faults have controlled the locations of some slump edges.
- A gas chimney that extends from just above potential source rocks to the Quaternary sequences is identified in the northeast of the study area. The base of the gas chimney is at the edge of a slump in an inferred extensional setting. Gas chimneys and intra-slump faulting could be the main controls for vertical migration of fluids from Miocene strata to Quaternary reservoirs, where major faults are not observed.

Acknowledgements

We thank Ministry of Economy, Trade and Industry Japan (METI) and Japan Oil, Gas and Metals National Corporation (JOGMEC) for providing the 3D seismic data acquired through METI Geophysical Survey and Basin Evaluation Project “Sanriku-Oki 3D”. We further thank Japan Agency for Marine-Earth Science and Technology (JAMSTEC) for providing the 2D seismic and logging data. We are grateful to O. Takano (JAPEX) for valuable discussions, associate editor D. Praeg, and T.M. Alves and D. Gamboa for constructive reviews of the manuscript. We gratefully acknowledge the support of the Japan International Cooperation Agency, and International Institute for Carbon-Neutral Energy Research sponsored by the World Premier International Research Center Initiative (WPI), MEXT, Japan.

References

Alves, T.M., Kurtev, K., Moore, G.F., Strasser, M., 2014. Assessing the internal character, reservoir potential, and seal competence of mass-transport deposits using seismic texture: a geophysical and petrophysical approachMass-Transport Deposits and Seismic Texture. AAPG Bull. 98 (4), 793–824.

Andreassen, K., Nilssen, E.G., Ødegaard, C.M., 2007. Analysis of shallow gas and fluid migration within the Plio-Pleistocene sedimentary succession of the SW Barents Sea continental margin using 3D seismic data. Geo Mar. Lett. 27 (2–4), 155–171.

Aqrawi, A.A., Weinzierl, W., Daber, R., Boe, T.H., 2012. Directional guided seismic attributes and their use in assisting structural, stratigraphic and lithological interpretation. In: SEG Technical Program Expanded Abstracts 2012. Society of Exploration Geophysicists, pp. 1–5.

Baba, K., Yamada, Y., 2004. BSRs and associated reflections as an indicator of gas hydrate and free gas accumulation: an example of accretionary prism and forearc basin system along the Nankai Trough, off central Japan. Resour. Geol. 54, 11–24.

Bale, S., Alves, T.M., Moore, G.F., 2014. Distribution of gas hydrates on continental margins by means of a mathematical envelope: a method applied to the interpretation of 3D Seismic Data. G-cubed 15 (1), 52–68.

Bangs, N.L.B., Sawyer, D.S., Golovchenko, X., 1993. Free gas at the base of the gas hydrate zone in the vicinity of the Chile triple junction. Geology 21 (10), 905–908.

Berndt, C., Mienert, J., Vanneste, M., Bünz, S., Bryn, P., 2002. May. Submarine slope-failure offshore Norway triggers rapid gas hydrate decomposition. In: Proceedings of the Fourth International Conference on Gas Hydrates, Yokohama, Japan, 19–23, May, pp. 71–74.

Bull, S., Cartwright, J., Huuse, M., 2009. A review of kinematic indicators from mass-transport complexes using 3D seismic data. Mar. Petrol. Geol. 26 (7), 1132–1151.

Cartwright, J., 2007. The impact of 3D seismic data on the understanding of compaction, fluid flow and diagenesis in sedimentary basins. J. Geol. Soc. 164 (5), 881–893.

Chhun, C., Kioka, A., Jia, J., Tsuji, T., 2018. Characterization of hydrate and gas reservoirs in plate convergent margin by applying rock physics to high-resolution seismic velocity model. Mar. Petrol. Geol. 92, 719–732.

Chi, W., Reed, D.L., Tsai, C., 2006. Gas hydrate stability zone in offshore southern Taiwan. Terr. Atmos. Ocean Sci. 17 (4), 829.

Chow, J., Lee, J.S., Sun, R., Liu, C.S., Lundberg, N., 2000. Characteristics of the bottom simulating reflectors near mud diapirs: offshore southwestern Taiwan. Geo Mar. Lett. 20 (1), 3–9.

Claypool, G.E., Kaplan, I.R., 1974. The origin and distribution of methane in marine sediments. In: Natural Gases in Marine Sediments. Springer, Boston, MA, pp. 99–139.

Crutchley, G.J., Fraser, D.R.A., Pecher, I.A., Gorman, A.R., Maslen, G., Henrys, S.A., 2015. Gas migration into gas hydrate-bearing sediments on the southern Hikurangi margin of New Zealand. J. Geophys. Res. 120 (2), 725–743.

Davis, E., Hyndman, R., Villinger, H., 1990. Rates of fluid expulsion across the northern cascadia accretionary prism: contraints from new heat flow and multichannel seismic reflection data. J. Geophys. Res. 95, 8869–8889.

Dorigo, M., Maniezzo, V., Colorni, A., 1996. Ant system: optimization by a colony of cooperating agents. IEEE Transactions on Systems, Man, and Cybernetics, Part B (Cybernetics) 26 (1), 29–41.

Dugan, B., 2012. Petrophysical and consolidation behavior of mass transport deposits from the northern Gulf of Mexico, IODP Expedition 308. Mar. Geol. 315, 98–107.

Ecker, C., Dvorkin, J., Nur, A.M., 2000. Estimating the amount of gas hydrate and free gas from marine seismic data. Geophysics 65 (2), 565–573.

Flemings, P.B., Long, H., Dugan, B., Germaine, J., John, C.M., Behrmann, J.H., Sawyer, D., Expedition, I.O.D.P., 2008. Pore pressure penetrometers document high overpressure near the seafloor where multiple submarine landslides have occurred on the continental slope, offshore Louisiana, Gulf of Mexico. Earth Planet Sci. Lett. 269 (3), 309–325.

Gamboa, D., Alves, T.M., 2015. Three-dimensional fault meshes and multi-layer shear in mass-transport blocks: implications for fluid flow on continental margins. Tectonophysics 647–648, 21–32.

Gamboa, D., Alves, T., Cartwright, J., 2011. Distribution and characterization of failed (mega) blocks along salt ridges, southeast Brazil: implications for vertical fluid flow on continental margins. J. Geophys. Res.: Solid Earth 116 (B8). https://doi.org/10.1029/2011JB008357.

Gay, A., Lopez, M., Cochonat, P., Séranne, M., Levaché, D., Sermondadaz, G., 2006. Stacked oligocene–miocene turbiditic palaeochannels in the lower Congo basin. Mar. Geol. 226 (1), 25–40.

Glombitza, C., Adhikari, R.R., Riedinger, N., Gilhooly III, W.P., Hinrichs, K.U., Inagaki, F., 2016. Microbial sulfate reduction potential in coal-bearing sediments down tõ 2.5 km below the seafloor off Shimokita Peninsula, Japan. Front. Microbiol. 7, 1576.

Gong, C., Wang, Y., Hodgson, D.M., Zhu, W., Li, W., Xu, Q., Li, D., 2014. Origin and anatomy of two different types of mass–transport complexes: a 3D seismic case study from the northern South China Sea margin. Mar. Petrol. Geol. 54, 198–215.

Gross, D., Bechtel, A., Harrington, G.J., 2015. Variability in coal facies as reflected by organic petrological and geochemical data in Cenozoic coal beds offshore Shimokita (Japan)-IODP Exp. 337. Int. J. Coal Geol. 152, 63–79.

Guan, Z., Chen, K., He, M., Zhu, J., Zhou, F., Yu, S., 2016. Recurrent mass transport deposits and their triggering mechanisms in the Kaiping Sag, Pearl river mouth basin. Mar. Petrol. Geol. 73, 419–432.

Haacke, R.R., Westbrook, G.K., Hyndman, R.D., 2007. Gas hydrate, fluid flow and free gas: Formation of the bottom-simulating reflector. Earth Planet Sci. Lett. 261, 407–420.

Holbrook, W.S., Hoskins, H., Wood, W.T., Stephen, R.A., Lizarralde, D., 1996. Methane hydrate and free gas on the Blake Ridge from vertical seismic profiling. Science 273 (5283), 1840–1843.

Husse, M., Feary, D.A., 2005. Seismic inversion for acoustic impedance and porosity of cenozoic cool-water carbonates on the upper continental slope of the Great Australian Bight. Mar. Geol. 215, 123e134.

Hyndman, R.D., Spence, G.D., 1992. A seismic study of methane hydrate marine bottom simulating reflectors. J. Geophys. Res. 97, 6683–6698.

Ijiri, A., et al., 2018. Deep-biosphere methane production stimulated by geofluids in the Nankai accretionary complex. Science Advances 4 (6), eaao4631. https://doi.org/10.1126/sciadv.aao4631.

Inagaki, F., Hinrichs, K.-U., Kubo, Y., the Expedition 337 Scientists, 2012. Deep coalbed biosphere off Shimokita: microbial processes and hydrocarbon system associated with deeply buried coalbed in the ocean. IODP Preliminary Report. https://doi.org/

10.2204/iodp.pr.337.2012.
Inagaki, F., Hinrichs, K.-U., Kubo, Y., the Expedition 337 Scientists 337, 2013. Proc. IODP, 337:Tokyo (Integrated Ocean Drilling Program Management International, Inc.). https://doi.org/10.2204/iodp.proc.337.101.2013.
Inagaki, F., Hinrichs, K.U., Kubo, Y., 2016. IODP Expedition 337: deep Coalbed Biosphere off Shimokita–Microbial processes and hydrocarbon system associated with deeply buried coalbed in the ocean. Sci. Drill. 21, 17–28.
Itoh, Y., Tsuru, T., 2006. A model of late Cenozoic transcurrent motion and deformation in the fore-arc of northeast Japan: constraints from geophysical studies. Phys. Earth Planet. In. 156 (1–2), 117–129.
Jia, J., Tsuji, T., Matsuoka, T., 2016. Gas hydrate saturation and distribution in the Kumano forearc basin of the Nankai Trough. Explor. Geophys. 48 (2), 137–150.
Jin, Y.K., Lee, M.W., Kim, Y., Nam, S.H., Kim, K.J., 2003. Gas hydrate volume estimations on the South Shetland continental margin, Antarctic Peninsula. Antarct. Sci. 15 (2), 271–282.
Judd, A.G., 2003. The global importance and context of methane escape from the seabed. Geo Mar. Lett. 23 (3–4), 147–154.
Judd, A.G., Hovland, M., 1992. The evidence of shallow gas in marine sediments. Continent. Shelf Res. 12 (10), 1081–1095.
Judd, A.G., Hovland, M., Dimitrov, L.I., Garcia Gil, S., Jukes, V., 2002. The geological methane budget at continental margins and its influence on climate change. Geofluids 2 (2), 109–126.
Kanamori, H., 1971. Seismological evidence for a lithospheric normal faulting—the Sanriku earthquake of 1933. Phys. Earth Planet. In. 4 (4), 289–300.
Kawabata, K., Sakaguchi, A., Hamada, Y., Tsuji, T., Kitamura, Y., Saito, S., 2018. Thermal fluid migration in the Kumano forearc basin, Nankai Trough, estimated via vitrinite reflectance measurement. In: Byrne, T., Underwood, M.B., Fisher, D., McNeill, L., Saffer, D., Ujiie, K., Yamaguchi, A. (Eds.), Geology and Tectonics of Subduction Zones: a Tribute to Gaku Kimura, pp. 141–154. Geological Society of America Special Paper 534. https://doi.org/10.1130/2018.2534(09.
Kennett, J.P., Cannariato, K.G., Hendy, I.L., Behl, R.J., 2003. Methane Hydrates in Quaternary Climate Change: the Clathrate Gun Hypothesi. American Geophysical Union, pp. 1–9.
Kinoshita, M., Moore, G.F., Kido, Y.N., 2011. Heat flow estimated from BSR and IODP borehole data: implication of recent uplift and erosion of the imbricate thrust zone in the Nankai Trough off Kumano. G-cubed 12 (9). https://doi.org/10.1029/2011GC003609.
Koide, H., Kuniyasu, M., 2006. Deep unmineable coalbeds in Japan: potential CO 2 sink and untapped energy resource. In: Proceedings of the 8th International Conference on Greenhouse Gas Technologies. Elsevier, Oxford, CD-ROM.
Kokusho, T., 2000. Mechanism for water film generation and lateral flow in liquefied sand layer. Soils Found. 40 (5), 99–111.
Koson, S., Chenrai, P., Choowong, M., 2014. Seismic attributes and their applications in seismic geomorphology. Bulletin of Earth Sciences of Thailand 6 (1), 1–9.
Kret, K., Tsuji, T., Takano, O., 2018. Characterization of hydrate and gas reservoirs off Sanriku area from high-resolution seismic velocity. In: Proceeding of the 13th SEGJ International Symposium.
Kumar, D., Sen, M.K., Bangs, N.L., 2006. Seismic characteristics of gas hydrates at Hydrate Ridge, offshore Oregon. Lead. Edge 25 (5), 610–614.
Kvenvolden, K.A., 1993. Gas hydrates-geological perspective and global change. Rev. Geophys. 31, 173–187. https://doi.org/10.1029/93RG00268.
Kvenvolden, K.A., 1998. A primer on the geological occurrence of gas hydrates. In: Henriet, J.-P., Mienert, J. (Eds.), Gas Hydrates - Relevance to World Margin Stability and Climate Change. The Geological Society, London, pp. 9–30.
Lamarche, G., Joanne, C., Collot, J.Y., 2008. Successive, large mass-transport deposits in the south Kermadec fore-arc basin, New Zealand: the Matakaoa Submarine Instability Complex. G-cubed 9 (4). https://doi.org/10.1029/2007GC001843.
Leynaud, D., Mienert, J., Nadim, F., 2004. Slope stability assessment of the Helland Hansen area offshore the mid-Norwegian margin. Mar. Geol. 213 (1–4), 457–480.
Lin, C.C., Lin, A.T.S., Liu, C.S., Chen, G.Y., Liao, W.Z., Schnurle, P., 2009. Geological controls on BSR occurrences in the incipient arc-continent collision zone off southwest Taiwan. Mar. Petrol. Geol. 26 (7), 1118–1131.
Lin, Y.N.N., Sieh, K., Stock, J., 2010. Submarine landslides along the Malacca Strait-Mergui Basin shelf margin: insights from sequence-stratigraphic analysis. J. Geophys. Res.: Solid Earth 115 (B12). https://doi.org/10.1029/2009JB007050.
Lodolo, E., Camerlenghi, A., Madrussani, G., Tinivella, U., Rossi, G., 2002. Assessment of gas hydrate and free gas distribution on the South Shetland margin (Antarctica) based on multichannel seismic reflection data. Geophys. J. Int. 148 (1), 103–119.
López, C., Ojeda, G., 2006. Heat flow in the Colombian Caribbean from the bottom simulating reflector (BSR). CT&F-Ciencia, Tecnol. Futuro 3, 29–39.
Løseth, H., Gading, M., Wensaas, L., 2009. Hydrocarbon leakage interpreted on seismic data. Mar. Petrol. Geol. 26 (7), 1304–1319.
Lu, S., McMechan, G.A., 2002. Estimation of gas hydrate and free gas saturation, concentration, and distribution from seismic data. Geophysics 67 (2), 582–593.
MacKay, M.E., Jarrard, R.D., Westbrook, G.K., Shipboard Scientific Party of Ocean Drilling Program Leg 146, 1994. Origin of bottom-simulating reflectors: geophysical evidence from the Cascadia accretionary prism. Geology 22, 459–462.
Maruyama, S., Isozaki, Y., Kimura, G., Terebayashi, M., 1997. Paleogeographic maps of the Japanese islands: plate tectonic synthesis 750 MA to present. Isl. Arc 6, 121–142.
Maver, K.G., Rasmussen, K.B., 1995. January. Seismic inversion for reservoir delineation and description. In: Middle East Oil Show. Society of Petroleum Engineers. https://doi.org/10.2118/29798-MS.
Milkov, A.V., Claypool, G.E., Lee, Y.J., Xu, W., Dickens, G.R., Borowski, W.S., 2003. In situ methane concentrations at Hydrate Ridge, offshore Oregon: new constraints on the global gas hydrate inventory from an active margin. Geology 31 (10), 833–836.
Miyakawa, A., Saito, S., Yamada, Y., Tomaru, H., Kinoshita, M., Tsuji, T., 2014. Gas hydrate saturation at site C0002, IODP expeditions 314 and 315,in the Kumano basin, Nankai Trough. Isl. Arc 23, 142–156. https://doi.org/10.1111/iar.12064.
Morita, S., Nakajima, T., Hanamura, Y., 2012. Possible ground instability factor implied by slumping and dewatering structures in high-methane-flux continental slope. In: Submarine Mass Movements and Their Consequences. Springer, Dordrecht, pp. 311–320.
Nimiya, H., Ikeda, T., Tsuji, T., 2017. Spatial and temporal seismic velocity changes on Kyushu Island during the 2016 Kumamoto earthquake. Science Advances 3 (11), e1700813.
Noda, A., TuZino, T., Joshima, M., Goto, S., 2013. Mass transport-dominated sedimentation in a foreland basin, the Hidaka Trough, northern Japan. G-cubed 14 (8), 2638–2660.
Oda, H., 2003. Cretaceous and paleogene coals in Japan as source rocks of natural gas and petrolem. In: AAPG International Conference, pp. 1–5.
Osawa, M., Nakanishi, S., Tanahashi, M., Oda, H., 2002. Structure, tectonic evolution and gas exploration potential of offshore Sanriku and Hidaka provinces, Pacific Ocean, off northern Honshu and Hokkaido, Japan. J. Jpn. Assoc. Pet. Technol. 67, 38–49.
Panpichityota, N., Morley, C.K., Ghosh, J., 2018. Link between growth faulting and initiation of a mass transport deposit in the northern Taranaki Basin, New Zealand. Basin Res. 30 (2), 237–248.
Paull, C.K., Ussler, W., Dillon, W.P., 1991. Is the extent of glaciation limited by marine gas-hydrates? Geophys. Res. Lett. 18 (3), 432–434.
Paull, C.K., Ussler, W., Borowski, W.S., 1994. Sources of biogenic methane to form marine gas hydrates: in-situ production or upward migration. In: In: Sloan, E.D. (Ed.), International Conference on Natural Gas Hydrates 715. Annals of the New York Academy of Sciences, pp. 392–409.
Peters, K.E., Cassa, M.R., 1994. Applied source rock geochemistry: chapter 5. In: Magoon, L.B., Dow, W.G. (Eds.), "The Petroleum System – from Source to Trap" AAPG Memoir 60.
Petersen, C.J., Papenberg, C., Klaeschen, D., 2007. Local seismic quantification of gas hydrates and BSR characterization from multi-frequency OBS data at northern Hydrate Ridge. Earth Planet Sci. Lett. 255 (3–4), 414–431.
Pigott, J.D., Kang, M.H., Han, H.C., 2013. First order seismic attributes for clastic seismic facies interpretation: examples from the East China Sea. J. Asian Earth Sci. 66, 34–54.
Regalla, C., Fisher, D.M., Kirby, E., Furlong, K.P., 2013. Relationship between outer forearc subsidence and plate boundary kinematics along the Northeast Japan convergent margin. G-cubed 14 (12), 5227–5243.
Riboulot, V., Cattaneo, A., Sultan, N., Garziglia, S., Ker, S., Imbert, P., Voisset, M., 2013. Sea-level change and free gas occurrence influencing a submarine landslide and pockmark formation and distribution in deepwater Nigeria. Earth Planet Sci. Lett. 375, 78–91.
Schnürle, P., Hsiuan, T.H., Liu, C.S., 1999. Constrains on free gas and gas hydrate bearing sediments from multi-channel seismic data, offshore southwestern Taiwan. Petrol. Geol. Taiwan 33, 21–42.
Shanmugam, G., Bloch, R.B., Mitchell, S.M., Damuth, J.E., Beamish, G.W.J., Hodgkinson, R.J., Straume, T., Syvertsen, S.E., Shields, K.E., 1996. Slump and debris-flow dominated basin-floor fans in the North Sea: an evaluation of conceptual sequence-stratigraphical models based on conventional core data. Geological Society, London, Special Publications 103 (1), 145–176.
Sloan Jr., E.D., Koh, C., 2007. In: Clathrate Hydrates of Natural Gases, third ed. CRC Press.
Strasser, M., Stegmann, S., Bussmann, F., Anselmetti, F.S., Rick, B., Kopf, A., 2007. Quantifying subaqueous slope stability during seismic shaking: lake Lucerne as model for ocean margins. Mar. Geol. 240 (1–4), 77–97.
Sun, Y., Wu, S., Dong, D., Lüdmann, T., Gong, Y., 2012a. Gas hydrates associated with gas chimneys in fine-grained sediments of the northern South China Sea. Mar. Geol. 311, 32–40.
Sun, Q., Wu, S., Cartwright, J., Dong, D., 2012b. Shallow gas and focused fluid flow systems in the Pearl river mouth basin, northern south China sea. Mar. Geol. 315, 1–14.
Sun, Q., Alves, T., Xie, X., He, J., Li, W., Ni, X., 2017. Free gas accumulations in basal shear zones of mass-transport deposits (Pearl River Mouth Basin, South China Sea): an important geohazard on continental slope basins. Mar. Petrol. Geol. 81, 17–32.
Taira, A., et al., 2005. Technical report volume 2 : Shimokita area site survey : northern Japan trench seismic survey, northern Hounshu, Japan. 155pp. http://www.jamstec.go.jp/cdex/e/sciencesupport/pdf/technical-report2.pdf.
Takano, O., 2017. Intermittent formation, sedimentation and deformation history of cenozoic forearc basins along the northwestern Pacific margins as an indicator of tectonic scenarios. In: Dynamics of Arc Migration and Amalgamation-architectural Examples from the NW Pacific Margin. InTech. https://doi.org/10.5772/intechopen.68290.
Takano, O., Tsuji, Y., 2017. Fluvial to bay sequence stratigraphy and seismic facies of the Cretaceous to Paleogene successions in the MITI Sanriku-oki well and the vicinities, the Sanriku-oki forearc basin, northeast Japan. Isl. Arc 26 (4). https://doi.org/10.1111/iar.12184.
Takano, O., Itoh, Y., Kusumoto, S., 2013. Variation in forearc basin configuration and basin-filling depositional systems as a function of trench slope break development and strike-slip movement: examples from the Cenozoic Ishikari–Sanriku-oki and Tokai-oki–Kumano-nada forearc basins, Japan. In: Itoh, Y. (Ed.), Mechanism of Sedimentary Basin Formation: Multidisciplinary Approach on Active Plate Margins. InTech, Rijeka, Croatia, pp. 3–25 ISBN: 978–953–51-1193-1.
Taladay, K., Boston, B., Moore, G.F., 2017. Gas-in-place estimate for potential gas hydrate concentrated zone in the Kumano basin, Nankai Trough forearc, Japan. Energies 10 (10), 1552. https://doi.org/10.3390/en10101552.
Taner, M.T., Koehler, F., Sheriff, R.E., 1979. Complex seismic trace analysis. Geophysics 44 (6), 1041–1063.

Tanikawa, W., Tadai, O., Morita, S., Lin, W., Yamada, Y., Sanada, Y., Moe, K., Kubo, Y.S., Inagaki, F., 2016. Thermal properties and thermal structure in the deep-water coalbed basin off the Shimokita Peninsula, Japan. Mar. Petrol. Geol. 73, 445–461.
Tanioka, Y., Sataka, K., 1996. Fault parameters of the 1896 Sanriku tsunami earthquake estimated from tsunami numerical modeling. Geophys. Res. Lett. 23 (13), 1549–1552.
Tinivella, U., Accaino, F., 2000. Compressional velocity structure and Poisson's ratio in marine sediments with gas hydrate and free gas by inversion of reflected and refracted seismic data (South Shetland Islands, Antarctica). Mar. Geol. 164 (1–2), 13–27.
Tomaru, H., Fehn, U., Lu, Z., Takeuchi, R., Inagaki, F., Imachi, H., Kotani, R., Matsumoto, R., Aoike, K., 2009. Dating of dissolved iodine in pore waters from the gas hydrate occurrence offshore Shimokita Peninsula, Japan: 129I results from the D/V Chikyu shakedown cruise. Resour. Geol. 59 (4), 359–373.
Townend, J., 1997. Estimates of conductive heat flow through bottom-simulating reflectors on the Hikurangi and southwest Fiordland continental margins, New Zealand. Mar. Geol. 141, 209–220.
Tsuji, T., Tokuyama, H., Costa Pisani, P., Moore, G., 2008. Effective stress and pore pressure in the Nankai accretionary prism off the Muroto Peninsula, southwestern Japan. J. Geophys. Res.: Solid Earth 113, B11401. https://doi.org/10.1029/2007JB005002.
Tsuji, T., et al., 2012. Hydrothermal fluid flow system around the Iheya North Knoll in the mid-Okinawa Trough based on seismic reflection data. J. Volcanol. Geoth. Res. 213–214, 41–50. https://doi.org/10.1016/j.jvolgeores.2011.11.007.
Tsuji, T., Kawamura, K., Kanamatsu, T., Kasaya, T., Fujikura, K., Ito, Y., Tsuru, T., Kinoshita, M., 2013. Extension of continental crust by anelastic deformation during the 2011 Tohoku-oki earthquake: the role of extensional faulting in the generation of a great tsunami. Earth Planet Sci. Lett. 364, 44–58. https://doi.org/10.1016/j.epsl.2012.12.038.
Tsuji, T., Ashi, J., Strasser, M., Kimura, G., 2015. Identification of the static backstop and its influence on the evolution of the accretionary prism in the Nankai Trough. Earth Planet Sci. Lett. 431, 15–25. https://doi.org/10.1016/j.epsl.2015.09.011.
Tsuji, T., Ishibashi, J., Ishitsuka, K., Kamata, R., 2017. Horizontal sliding of kilometre-scale hot spring area during the 2016 Kumamoto earthquake. Sci. Rep. 7, 42947. https://doi.org/10.1038/srep42947.
Von Huene, R., Lallemand, S., 1990. Tectonic erosion along the Japan and Peru convergent margins. Geol. Soc. Am. Bull. 102 (6), 704–720.
Von Huene, R., Langseth, M., Nasu, N., Okada, H., 1982. A summary of Cenozoic tectonic history along the IPOD Japan Trench transect. Geol. Soc. Am. Bull. 93 (9), 829–846.
Xie, X., Heller, P.L., 2009. Plate tectonics and basin subsidence history. Geol. Soc. Am. Bull. 121 (1–2), 55–64.
Yamano, M., Uyeda, S., Aoki, Y., Shipley, T.H., 1982. Estimates of heat flow derived from gas hydrates. Geology 10 (7), 339–343.
Yu, X., Wang, J., Liang, J., Li, S., Zeng, X., Li, W., 2014. Depositional characteristics and accumulation model of gas hydrates in northern South China Sea. Mar. Petrol. Geol. 56, 74–86.